Characterizing severe weather potential in synoptically weakly forced thunderstorm environments

By

Paul W. Miller*

and

Thomas L. Mote

Department of Geography
University of Georgia, Athens, Georgia

*Corresponding author address: Department of Geography, 210 Field Street, Room 204 Athens, GA 30602. Email: paul.miller@uga.edu

Submitted as an article to *Natural Hazards and Earth System Sciences*

Submitted: 9 August 2017

Submitted with technical corrections: 6 October 2017

Submitted with revisions: 30 January 2018

Abstract

Weakly forced thunderstorms (WFTs), short-lived convection forming in synoptically quiescent regimes, are a contemporary forecasting challenge. The convective environments that support severe WFTs are often similar to those that yield only nonsevere WFTs, and additionally, only a small proportion of individual WFTs will ultimately produce severe weather. The purpose of this study is to better characterize the relative severe weather potential in these settings as a function of the convective environment. Thirty-one near-storm convective parameters for >200,000 WFTs in the Southeast United States are calculated from a high-resolution numerical forecasting model, the Rapid Refresh (RAP). For each parameter, the relative odds of WFT days with at least one severe weather event is assessed along a moving threshold. Parameters (and the values of them) that reliably separate severe-weather-supporting from nonsevere WFT days are highlighted.

Only two convective parameters, vertical totals (VT) and total totals (TT), appreciably differentiate severe-wind-supporting and severe-hail-supporting days from nonsevere WFT days. When VTs exceeded values between 24.6–25.1°C or TTs between 46.5–47.3°C, odds of severe-wind days were roughly 5x greater. Meanwhile, odds of severe-hail days became roughly 10x greater when VTs exceeded 24.4–26.0°C or TTs exceeded 46.3–49.2°C. The stronger performance of VT and TT is partly attributed to the more accurate representation of these parameters in the numerical model. Under-reporting of severe weather and model error are posited to exacerbate the forecasting challenge by obscuring the subtle convective environmental differences enhancing storm severity.

Keywords: weakly forced thunderstorms, pulse thunderstorms, storm environments, severe weather

1. Introduction

Weakly forced thunderstorms (WFTs), convection forming in synoptically benign, weakly sheared environments, are a dual forecasting challenge. Not only is the exact location and time of convective initiation difficult to predict, but once present, the successful differentiation of severe WFTs from their benign counterparts is equally demanding. Consequently, severe weather warnings issued on WFTs in the U.S. are less accurate than more organized storm modes, such as squall lines and supercells (Guillot et al., 2008). American operational meteorologists have coined these severe WFTs "pulse thunderstorms" because the surge of the updraft that produces the severe weather occurs in a brief "pulse" (Miller and Mote, 2017). The United States National Weather Service defines "severe weather" as any of the following: winds $\geq$ 26 m s^{-1}, hail $\geq$ 2.54 cm in diameter, or a tornado.

Environments thought to support pulse thunderstorms are typically characterized by weak vertical wind shear and strong convective available potential energy (CAPE). However, not all weak-shear, high-CAPE environments facilitate pulse thunderstorms, nor are all pulse thunderstorms confined to environments with the weakest shear and/or strongest instability. The result is a low signal-to-noise ratio (SNR) which obstructs the reliable discernment of pulse-supporting environments. The SNR is common discussion point in climate variability research where it often describes the relative magnitudes of a climate change trend (i.e., the signal) versus inter-annual variability (i.e., the noise) (e.g., Hamlington et al., 2010; Sutton and Hodson, 2007; Trenberth, 1984). In our context, the "signal" refers to the true difference between the large-scale convective environments that support severe weather and those that do not. Meanwhile, the "noise" represents the many processes than might cause storms to produce (not produce) severe weather in an environment where it was not expected (expected). Cell interactions, stabilization from prior

convection, surface convergence, locally enhanced shear, model error, etc, can act as noise in the operational setting.

Prior research directed at pulse thunderstorms is limited, and work has not typically included a representative proportion of nonsevere WFTs in their samples (Atkins and Wakimoto, 1991; Cerniglia and Snyder, 2002). If the sample contains too many pulse thunderstorms, the SNR may be artificially bolstered, results overstated, and the potential reliability in an operational setting diminished. For instance, in a meta-analysis of studies pertaining to new lightning-based storm warning techniques, Murphy (2017) found that the studies' reported false alarms ratios (FAR) were directly proportional to the fraction of nonsevere storms contained in the sample. Samples that included a realistic ratio of severe-to-nonsevere storms demonstrated the weakest skill scores.

Most research considering pulse thunderstorms in the Southeast U.S. has typically focused on one of its primary severe weather mechanisms: the wet microburst. Severe wet microbursts generally occur in atmospheres characterized by a deep moist layer extending from the surface to 4–5 km above ground level (Johns and Doswell, 1992). Above the moist layer lies a mid-level dry layer with lower equivalent potential temperature values (θ_e). In wet microburst environments, the difference between the maximum θ_e observed just above the surface and the minimum θ_e aloft exceeded 20 K, whereas non-microburst-producing thunderstorm days had differences less than 13 K (Atkins and Wakimoto, 1991; Roberts and Wilson, 1989; Stewart, 1991; Wheeler and Spratt, 1995). However, Atkins and Wakimoto (1991) examined only 14 microburst days versus three non-microburst days. Adding to the uncertainty, James and Markowski (2010) challenged the role of mid-level dry air in severe weather production. The results of their cloud-scale modeling

experiment indicated that, for all but the highest instabilities tested, drier mid-level air did not correspond to increased downdraft and cold pool intensity.

Building on these findings, several severe weather forecasting parameters have been developed to distill the atmosphere's vertical thermodynamic profile into a single value representing the damaging wind potential. McCann (1994) developed a microburst-predicting "wind index" (WINDEX) to be used in the forecasting of wet downburst potential. However, although WINDEX performed well when tested in known microburst environments, no null cases were presented (McCann, 1994). Additional severe wind potential indices include the wind damage parameter and the microburst index described by the United States Storm Prediction Center (SPC; http://www.spc.noaa.gov/exper/soundings/help/index.html). Tools such as total totals, k-index, the Severe WEAther Threat (SWEAT) index, etc, are also commonly used to forecast convective potential as well as the severity of thunderstorms.

However, the comparative utility of these environmental parameters within weakly forced regimes is unclear, particularly when they are tested with a realistic proportion of severe storms. Many of the results above were obtained by analyzing relatively small datasets, and they have not been tested against each other in a weakly forced environment. Therefore, this study seeks to compare the relative skill of convective parameters using a large WFT dataset to determine which are most appropriate for detecting environments supportive of pulse-thunderstorm-related severe weather.

2. Data and Methods

2.1 WFT selection and environmental characterization

This study uses the 15-yr WFT dataset developed by Miller and Mote (2017) for the Southeast U.S. (Fig. 1). Their detection method first identifies thunderstorms as regions of spatiotemporally contiguous composite reflectivities meeting or exceeding 40 dBZ using connected neighborhoods labeling. Each thunderstorm is then assigned five morphological attributes describing it shape, duration, intensity, etc, and all thunderstorms are clustered into ten morphologically similar groups using Ward's clustering (Ward, 1963). The composite convective environments associated with each morphological group were characterized using radiosonde observations from three launch sites in the Southeast U.S. WFTs were designated as the subset of morphological groups with small, short-lived, diurnally driven thunderstorms that also formed in weak-shear, strong-instability composite environments. Table 1 provides the composite kinematic and thermodynamic environmental characteristics for the ten morphological groups from Miller and Mote (2017). The WFTs are spatially referenced according to their first-detection location, the centroid of the composite reflectivities constituting the first appearance on radar. The storms were then paired with severe weather reports from *Storm Data*, a storm event database maintained by the United States National Centers of Environmental Information, to differentiate benign WFTs from pulse thunderstorms. The entire 15-yr dataset contains 885,496 WFTs including 5316 pulse thunderstorms.

Meanwhile, the thermodynamic and kinematic environment of each WFT was characterized using the 0-hr Rapid Refresh (RAP) analysis. The RAP, implemented on 9 May 2012, is a 13-km non-hydrostatic weather model initialized hourly for the purpose of near-term mesoscale forecasting which is operated by the United States National Center for Environmental Prediction. The RAP uses the National Oceanic and Atmospheric Administration (NOAA) Gridpoint Statistical Interpolation (GSI) system to assimilate radar reflectivity, lightning flashes

(added in version 3), radiosonde observations, GOES cloud analysis, wind profiler data, surface station observations, etc. Lateral boundary conditions are provided by the Global Forecast System (GFS). Additional information regarding the RAP assimilation system and model physics can be found in (Benjamin et al., 2016). The model has output available at 37 vertical levels spaced at 25-hPa intervals between 1000 and 100 hPa and 10-hPa intervals above 100 hPa. Several previous studies have relied upon the RAP's predecessor, the Rapid Update Cycle (RUC; Benjamin et al., 2004), to effectively characterize near-storm environments differentiating supercellular versus non-supercellular and tornadic versus non-tornadic thunderstorms (Thompson et al., 2007; Thompson et al., 2014).

For the grid cell containing each WFT's first-detection location, a RAP proxy sounding was created using the SHARPpy software package (Blumberg et al., 2017). Thus, each proxy sounding represents the model-derived storm environment for a point no more than 13 km and 30 min distant from the WFT first-detection location. The proxy soundings were used to calculate 31 near-storm environmental variables and indices, a complete list of which is provided in Table 2 with more thorough descriptions in Appendix A. The 31 variables were largely selected by virtue of their accessibility in SHARPpy. Four warm seasons of the Miller and Mote (2017) dataset, containing 228,363 WFTs and 1481 pulse thunderstorms, overlapped with the RAP's operational archive period allowing >6 million near-storm parameters to contribute to the analysis.

2.2 RAP error assessment

Thompson et al. (2003) demonstrated the suitability of the RUC, version 2 (RUC-2), to represent storm environments as evaluated using co-located radiosonde observations, and the Benjamin et al. (2016) RAP validation statistics show that the RAP is more accurate than its

predecessor. Figure 2a shows the results of an error evaluation specific to the purposes of this study. Vertical error profiles were calculated for 3562 co-located RAP predictions and observed radiosonde profiles in the Southeast U.S. The comparisons contain 0000 and 1200 UTC soundings during the warm season (May–September) between 2012 and 2015 at three launch sites along a north-south trajectory through the Miller and Mote (2017) domain: Nashville, Tenn., Peachtree City, Ga., and Tampa, Fla., corresponding to U.S. radar identification codes KOHX, KFFC, and KTBW in Fig. 1. The synoptic station codes for these three sites are the same as their U.S. radar identifications with the exception of Nashville, Tenn., whose synoptic code is KBNA.

Similar to the Thompson RUC-2 analysis, the greatest, albeit small, temperature and moisture biases (mean errors) from the RAP reside near the surface and the upper atmosphere (Fig. 2a). Aided by the large sample of comparison soundings, the 95% confidence intervals indicate that the true bias of the selected RAP output variables at these sites can be estimated with reasonable confidence. The 95% mixing ratio confidence interval captures zero at all altitudes except 500 hPa, where the RAP predicted drier-than-observed values by 0.08 g kg^{-1}. Temperatures are warmer than observed throughout most of the troposphere with a maximum bias of 0.26°C at 850 hPa. In contrast, the RAP underestimated wind speeds on average throughout the depth of the troposphere. The largest bias, 0.46 m s^{-1}, was found at 925 hPa with similar errors above 500 hPa. The 95% confidence interval for wind speed error is largest near the tropopause, and demonstrates larger uncertainty than for temperature and mixing ratio. These results generally agree with the error statistics provided by Benjamin et al. (2016), and the reader should reference that paper for additional information, including validation statistics, about the RAP.

Although the RAP appears to resolve temperature, mixing ratios, and wind speeds more accurately than the RUC-2, the transmission of these errors onto the derived convective parameters

182 can be large. Table 3 expresses error measures for surface-based (SBCAPE) and mean-layer CAPE
183 (MLCAPE), 0–3-km and 0–6-km wind shear, total totals, and the theta-e index. Because the focus
184 of this study is surface-based convection, only days when the observed surface-based CAPE was
185 greater than zero were used to calculate the derived quantity error metrics. Similar to previous
186 work (e.g., Lee, 2002), parameters calculated via the vertical integration of a parcel trajectory,
187 such as CAPE, are sensitive to errors in low-level temperature and moisture. The RAP's low-level
188 temperature and moisture biases influence the lifted condensation level (LCL) calculation
189 (negative MLLCL bias; Table 3) yielding a premature transition to the pseudo-adiabatic lapse rate
190 and an overestimate of parcel instability (positive SBCAPE and MLCAPE biases; Table 3)[1].
191 Thompson et al. (2003) identified smaller CAPE errors generated by the RUC-2; however, the
192 nature of the thermodynamic environments being examined is significantly different in this study.
193 Similar to the RUC-2, the RAP is more adept at representing MLCAPE than SBCAPE with Fig.
194 2b, and consequently, the mean-layer parcel trajectory will be used for all parcel-related
195 calculations.

196 In some cases, RAP proxy soundings may have been contaminated by premature
197 convective overturning within the model. However, because the RAP assimilates radar reflectivity
198 from the U.S. (Benjamin et al., 2016), the 0-hr RAP analysis fields should generally mirror the
199 radar-observed areas of convection. Additionally, any such instances will be dampened by the
200 methodological design decision to aggregate all proxy soundings on a daily level as will be
201 described in Sect. 2.3. The accuracy of the proxy soundings could be improved by employing a
202 convection-permitting numerical model, such as the 3-km High-Resolution Rapid Refresh

[1] The near-surface temperature and moisture errors in Fig. 2a are more pronounced following the upgrade to RAPv2 in February 2014. However, because the RAP is an operational tool and this work has operational relevance, no attempt was made to correct for this change.

(HRRR). By explicitly modeling deep convection, the HRRR would limit convective contamination by more closely representing areas of thunderstorm activity. At the time of publication, the absence of a publicly accessible HRRR archive prevented its application in this research.

Figures 2b-d demonstrate that although large outliers certainly occur, the majority of RAP-derived thermodynamic and kinematic parameters are concentrated within a narrower range of error. Figure 3 provides an example skewT-logP diagram for a large MLCAPE error shown in Figure 2d. Though the difference in this case exceeded 1000 J kg^{-1}, the discrepancy can largely be attributed to the RAP's minor mischaracterization of low-level moisture. Otherwise, the depiction of the vertical profile is reasonably accurate. The advantage of the RAP to represent the near-storm environment is underscored when compared to results from coarser-scale models. For instance, the coefficients of determination (R^2) for RAP-derived SBCAPE and MLCAPE are appreciably larger than those calculated from the 32-km horizontal and 3-hr temporal resolution North American Regional Reanalysis (NARR; Mesinger et al., 2006) in Gensini et al. (2014).

2.3 Assessing convective parameter skill

The quality of severe weather reports is a significant impediment to severe storm research (e.g., Miller et al., 2016; Weiss et al., 2002), particularly regarding the certainty with which nonsevere storms can be declared nonsevere. These storms may only appear benign because their associated severe weather was not reported. Consequently, the results of the proxy soundings are subdivided by nearest radar site (Fig. 1) and aggregated daily (1200–1200 UTC) by computing the mean parameter value associated with all WFTs forming within each polygon on a given day. Days containing at least one severe weather report are considered supportive of severe weather whereas

days with no severe weather reports will serve as the control. This approach is similar to the methods the Hurlbut and Cohen (2013) study of severe thunderstorm environments in the Northeast U.S. Severe-wind-supporting (SWS) days and severe-hail-supporting (SHS) days are treated separately because their thermodynamic environments have been shown to contain unique elements related to downdraft and hailstone production (Johns and Doswell, 1992). Table 4 provides the specific subdivision details of the frequency of WFT days, SWS days, SHS days, and their respective control days. Figure 4 shows the annual average of WFT days for each radar site within the study area during the 2012–2015 warm seasons. As expected, WFT days are most frequent along coastlines and the Appalachian Mountains (Miller and Mote, 2017).

Given the low SNR in WFT environments, *t*-tests are deceiving. Statistically significant differences in the mean values of parameters on severe versus nonsevere days are routinely reported, but the considerable overlap between the distributions (e.g., Craven and Brooks, 2004; Taszarek et al., 2017) can remove much practical value. This study explores the relationship between convective parameters and pulse thunderstorm environments by means of an odds ratio (OR; e.g., Fleiss et al., 2003). The OR is a common measure of conditional likelihood in human health and risk literature (e.g., Bland and Altman, 2000) with precedence in the atmospheric sciences (e.g., Black and Mote, 2015; Black et al., 2017). The OR looks past the descriptive statistics of the severe versus nonsevere distributions and more directly compares differences in where the data are concentrated within the distributions.

Equation 1 shows the standard definition of the OR, essentially the ratio of two ratios,

$$OR = \frac{A/C}{B/D} \tag{1}$$

where the numerator represents the ratio of events (A) to non-events (C) when a condition is met whereas the denominator is the ratio of events (B) to non-events (D) when the same condition is

not satisfied. In this context, "events" are SWS or SHS days whereas "non-events" would be the respective control days. Higher ORs indicate that events are more frequent (relative to non-events) when the condition is met, or conversely, that events are less frequent when the condition is not met. For this study, a condition might be a convective parameter exceeding a specified threshold. For instance, if the SWS OR equals 4 for the condition MLCAPE > 1000 J kg^{-1}, then the odds of an SWS day are 4x greater when MLCAPE is greater than 1000 J kg^{-1} than when it is less than 1000 J kg^{-1}.

We employ a modified form of the OR in which both the numerator and denominator are standardized by the climatological ratio of events to non-events (Eq. 2), allowing the components of the OR to be separated and interpreted independently by comparison to climatology.

$$OR = \frac{\frac{A/C}{(A+B)/(C+D)}}{\frac{B/D}{(A+B)/(C+D)}} \quad (2)$$

The modification does not change the value of the quotient OR, but it does improve the interpretability of the numerator and denominator. When the numerator or denominator is near zero (one), then the odds of SWS or SHS days are much lower than (nearly equal to) climatology. The climatological odds ratio was 0.069 for SWS days and 0.025 for SHS days. A 95% confidence interval for the OR was calculated using the four-step method presented in Black et al. (2017).

3. Results

3.1 Convective environments of pulse thunderstorm wind events

During the four-year study period, pulse thunderstorm wind events were documented somewhere in the study area on 49% of WFT days, although the average frequency within any

single subdivision was 6.7% (Table 4). Table 5 shows the 31 convective parameters analyzed from the proxy soundings as well as the number of subdivisions for which each parameter is a statistically significant differentiator of SWS days. A significance threshold of $p < 0.10$ guided the selection of potentially useful parameters which would be examined in more detail. Nine of the 31 variables are statistically significant across at least two-thirds of the study area: VT, TT, MLCAPE, MLLCL, MICROB, DCAPE, TEI, RH_LOW, and ThE_LOW.

Figure 5a-h depicts the distributions for several parameters from Table 5 for control versus SWS days. These eight parameters are either significant across much of the domain (VT and TT), demonstrate larger relative changes on SWS days (MLCAPE and MLLCL), and/or are traditional operational severe wind forecasting tools (DCAPE, TEI, WNDG, MICROB). However, as the distributions clearly illustrate, any difference in the mean values between the control days and SWS days is small compared to the spread about their means. This results in the characteristically low SNR described in the Sect. 1. Any attempt to establish a forecasting value indicative of pulse-wind potential will yield many missed events occurring beneath the threshold and/or false alarms associated with control days above it.

Thus, Fig. 6 employs the OR to characterize the relative skill that some knowledge of the convective environment can contribute to a severe versus nonsevere designation. For each variable in Fig. 5, a progressively larger value is selected, and the OR is calculated at each step. Figure 6 displays the OR as well as both the numerator and denominator terms for each iteration. High ORs can often result when a near-zero number of severe events exist below the threshold inflating the OR calculation. In these situations, the OR is indicating that severe weather is very unlikely, rather than that the severe weather risk is enhanced. These results are not particularly useful because forecasters would not have needed a decision-support tool in these environments in the first place.

Ideally, large ORs will result when the numerator indicates an appreciable increase against the climatology while the denominator simultaneously indicates an appreciable decrease below climatology. Further, these ORs would ideally occur in a range where the severe weather risk may be uncertain. In Fig. 6, the OR is shown in a gray line, but the line is drawn in black whenever the OR results from a numerator ≥ 2 and a denominator ≤ 0.5. ORs resulting from this combination indicate that the threshold yields a simultaneous two-fold increase (decrease) in the odds of SWS days above (below) the specified value. These ORs will be hereon referenced as "two-fold" ORs, and represent a goal scenario.

Figures 6a-h show ORs for the same eight parameters in Fig. 5. Of all eight parameters, only VT and TT achieve two-fold ORs for any range of thresholds, as indicated by the black segments in Fig. 6a-b. The maximum two-fold OR for VT is 5.16 at 24.6°C, meaning that the odds of an SWS day are 5.16x greater when this threshold is met. TT offers slightly more skill with a maximum two-fold OR of 5.70 at 46.5°C. As described in Appendix A, VT (vertical totals) and TT (total totals) are relatively primitive indices. VT is purely a temperature lapse rate whereas TT is predominantly a measure of lapse rate with an additional dewpoint term included. Meanwhile, MLCAPE and MLLCL demonstrate consistently lower ORs between 2 and 4. The four wind-specific variables in Fig. 6e-h are relatively poor differentiators of SWS days in the WFT regime. The maximum OR achieved by any of these parameters is approximately 10 driven by very low values of DCAPE with corresponding wide confidence intervals.

Though ORs are greater at lower VT and TT thresholds, these values are also somewhat common. Placing the aforementioned values (24.6°C and 46.5°C, respectively) in the context of the 12,759 WFT environments included in this study, they represent the 58.8^{th} and 58.9^{th} percentiles of their distributions. Alternatively, the maximum VT threshold that yields a two-fold

OR is 25.1°C, which corresponds to the 70.9th percentile of all VTs in the dataset; however, the OR for this value is smaller, 4.77. This result illustrates the trade-off involved by seeking climatologically exceptional values to serve as guidance. As greater values are selected as the threshold, meteorologists can focus on a fewer number of days. However, the OR decreases as more severe weather events occur in environments not satisfying the threshold. As for TT, the maximum two-fold OR value is 47.3°C, corresponding to the 70.6th percentile, but demonstrates an OR of 5.16. This means that when TT meets or exceeds 47.3°C, the odds of a pulse thunderstorm severe wind event are 5.16x greater than when it does not.

3.2 Convective environments of pulse thunderstorm hail events

Table 6 replicates Table 5 except for SHS days. Many of the same parameters that are statistically significant differentiators of SWS days also rank high for SHS days. However, fewer parameters in Table 6 are statistically significant over two-thirds of the domain. Whereas 10 parameters in Table 5 showed spatially expansive statistical skill on SWS days, only three quantities do so on SHS days. We attribute this result to the pattern in Table 4 and Fig. 4b-c whereby there are fewer SHS days than SWS days, which increases uncertainty related to the statistical tests and makes it harder to confidently detect differences.

Nonetheless, VT and TT are once again skillful differentiators, and are now joined by their related parameter CT. Additionally, several new convective variables demonstrate statistical significance across roughly half of the domain on SHS days that demonstrated little skill on SWS days: PW, PEFF, HGT0, and ApWBZ. For comparison, Fig. 7a-d duplicates Fig. 5a-d now comparing distributions between the control and SHS days while Fig. 7e-h displays boxplots for the SHS-specific convective parameters listed above. The distributions for MLCAPE and MLLCL

are similar; however, there is a larger separation between control and SHS days for VT and TT than was apparent on SWS days. This observation is corroborated by the relative changes in VT and TT on SHS days that are several percentage points larger than for SWS days (Table 6). PW, PEFF, HGT0, and ApWBZ demonstrate smaller differences.

Figure 8 replicates Fig. 6 except by representing SHS days and substituting the four wind-specific parameters (DCAPE, TEI, WNDG, MICROB) with the four hail parameters listed above (PW, PEFF, HGT0, ApWBZ). The ORs for VT and TT are large, greater than 10, throughout the entire range of thresholds tested, and contain larger swathes of two-fold ORs. The maximum two-fold OR for VT is 13.1 at 24.4°C, and the maximum VT threshold that achieves a two-fold OR is 26.0°C with an OR of 9.61. These values relate to the 53.4^{th} and 86.0^{th} percentiles of the VT distribution. As for TT, the maximum two-fold OR is 14.98 at 46.3°C, and the maximum two-fold-OR threshold is 49.2°C with an OR of 11.79. These two TT cut-offs translate to the 55.7^{th} and 88.4^{th} percentiles. Similar to SWS days, MLCAPE and MLLCL show little skill with ORs generally between 1–2. PW, PEFF, HGT0, and ApWBZ perform more capably than MLCAPE and MLLCL; however, they do not produce any two-fold ORs. Values for these metrics are generally around 4 with several instances of higher ORs driven by a small denominator with wide 95% confidence intervals.

3.3 Separating marginal pulse thunderstorm days

Because the severe weather generated by pulse thunderstorms is often near the lower limit used to define severe weather in the United States, some pulse thunderstorm environments may closely resemble nonsevere regimes. Consequently, the influence of these "marginal" pulse thunderstorm days on the OR analysis is further scrutinized. For this purpose, "marginal" SWS

and SHS days are defined as those on which only one severe wind or hail report was received. Marginal days constitute 48.7% of the SWS days and 57.7% of the SHS days in Table 4. Figure 9 replicates the OR analysis for VT and TT, the two most promising environmental parameters from Sects. 3.1 and 3.2, but with only marginal SWS and SHS days being considered. Comparing Figs. 6a-b and 8a-b to Fig. 9, marginal SWS and SHS days resemble the OR patterns of the broader set of SWS (Fig. 6a-b) and SHS (Fig. 8a-b) days. Though the ORs for the marginal subset are slightly smaller than for the broader group, they bear similar OR patterns as the thresholds are increased. Overall, marginal SWS and SHS days are generally characterized by similar VT and TT values as when all SWS and SHS days were aggregated. Corroborating this finding, an OR analysis comparing marginal SWS and SHS days to those with >1 severe event (not shown) revealed that ORs generally remained near 1 regardless of the VT or TT threshold selected. Thus, although marginal pulse thunderstorm days are by no means easily distinguishable from non-severe WFT days, they do not appear to be particularly more challenging to differentiate than active pulse thunderstorm days.

4. Discussion

The relative changes in the convective variables in Table 5 on SWS days versus control days correspond well to previous microburst research. Compared to the nonsevere control days, SWS days are characterized by a drier near surface layer (i.e., lower RH, higher LCLs). Simultaneously, steep mid-level lapse rates (i.e., larger VT and TT) aid an increase in CAPE which supports stronger updrafts. As the strong updraft transitions to a downdraft-dominant storm, the drier surface layer supports evaporative cooling, downdraft acceleration, and severe outflow

winds. This same conceptual model has been promoted by previous severe convective wind research (e.g., Atkins and Wakimoto, 1991; Kingsmill and Wakimoto, 1991; Wolfson, 1988).

The results of SHS days also support previous findings (Johns and Doswell, 1992; Moore and Pino, 1990; Púčik et al., 2015). The distributions in Fig. 7 (and relative changes in Table 6) indicate that SHS days are characterized by relative decreases in PW, a lower freezing level, a lower wet-bulb freezing level, and dry near-surface air. Smaller PWs result in less waterloading and greater parcel buoyancy (larger VT, TT, and MLCAPE) which maximizes updraft strength. Meanwhile, lower freezing levels and a dry layer between 1000–850 hPa support evaporative cooling which can together yield a lower wet-bulb zero height and limit hail stone melting during its descent to the surface. Interestingly, these two concepts are both represented in the PEFF calculation (Appendix A) which was not developed as a hail indicator. PEFF as defined by Noel and Dobur (2002), equals the product of PW and the mean 1000–700-hPa RH. As both values decrease, PEFF becomes smaller and hail is more likely for the reasons stated above.

The poor performance of MLLCLs and MLCAPEs in differentiating SWS and SHS days from their controls is surprising given their prominence in severe storm forecasting. One possibility is that the daily aggregation of MLCAPEs may have smoothed out locally higher values near the WFTs that were responsible for severe weather production. Alternatively, VT and TT were among the strongest indicators of both SWS and SHS days. Recalling from Sect. 2.2, VT and TT are also very well represented by the RAP. TTs were replicated by the model with a <1°C bias and a MAE representing only 3% of the average value (Table 3). Additionally, mid-level temperatures, from which VT is computed, also compared very well to the observed soundings (Fig. 2a). The strong performance of VT and TT compared to other more heavily moisture-weighted metrics may be due to their more accurate representation in the proxy soundings.

Regardless, because the severe weather SNR is already low in WFT environments, any systematic error introduced by the data source (in this case the RAP) may significantly dampen, or even remove, whatever environmental differences exist. As Sect. 2.2 indicated and previous work has also concluded, low-level moisture biases can impede the accurate calculation of convective parameters relying on those terms (e.g., Gensini et al., 2014; Thompson et al., 2003). In this study, MLCAPE, MLLCL, PW, PEFF, and others were vulnerable to such errors. The poorer performance of these variables' ORs (relative to the lapse-rate-based parameters) and the sensitivity of PW, PEFF, and ApWBZ to simulated RAP errors suggests that model inaccuracies may be obscuring their potential skill to detect weakly forced severe weather environments. The perception of the WFT environment as a difficult-to-forecast regime may partly be driven by model inconsistency exacerbating an already small SNR.

Another confounding factor is the quality of the *Storm Data* severe weather reports. Section 3.3 discussed that marginal SWS and SHS days are more similar to days with >1 report than days with no reports. Thus, the basis for the similarity may be that severe weather was simply under-reported on "marginal" days. Extending this logic, the pulse regime's low SNR may also be partially attributed to under-reporting of severe weather on "nonsevere" days. Given that the severe weather generated by pulse convection is often short-lived, isolated, and narrowly exceeds severe criteria, the notion that some pulse-related severe weather events go undetected is likely. If some "nonsevere" days existing above the tested parameter thresholds in Figs. 6 and 8 did in fact host severe weather, then the ORs would have been larger than those found in Sects. 3.1 and 3.2.

5. Conclusions

Hazardous weather within WFT environments is characterized by a lower SNR than other severe thunderstorm regimes. Though past research has developed promising tools for forecasting pulse thunderstorm environments, their relatively small samples sizes may have understated the SNR, and by corollary overstated the reliability of their tools. With recent research suggesting that the performance of new severe weather forecasting tools is closely tied to the proportion of nonsevere thunderstorms in the sample (Murphy, 2017), this study sought to test the relative skill of 31 convective forecasting parameters using realistic proportions of severe and nonsevere WFT environments (severe: 7.9%; nonsevere: 92.1%). Future research may consider broadening the methods of Murphy (2017) to standardize the skill values across previous studies of severe convective environments.

Only 13 (5) of the 31 convective parameters tested were statistically significant ($p < 0.10$) differentiators of SWS (SHS) days across at least half of the domain. Though the distinctive variables for SWS and SHS days were consistent with previous theories of severe microburst and hail formation, considerable overlap between the distribution of values on severe and nonsevere days is problematic. Similarities between the SWS, SHS, and their corresponding control distributions inhibit consistent identification of pulse thunderstorm potential based on the value of any individual parameter. Nonetheless, VT and TT did perform more skillfully than the others. When VTs exceed values between 24.6–25.1°C or TTs between 46.5–47.3°C, the relative odds of a wind event increases roughly 5x. Meanwhile, the odds of a hail event become roughly 10x greater when VTs exceed values between 24.4–26.0°C or TTs between 46.3–49.2°C.

The noteworthy performance of VT and TT, two quantities calculated from the more reliable RAP output fields, is unlikely a coincidence. Our findings suggest that the already weak

severe weather SNR in WFT environments is exacerbated by model limitations in the low-level moisture and temperature fields. Meteorologists may perhaps alleviate the challenges of the WFT environment by examining convective parameters that are well-represented by models, such as VT, TT, and other measures of lapse rate. Future research might seek to track the transmission of the model errors through calculation of forecast skill statistics, and more concretely ascertain the contribution of model error to the SNR.

6. Acknowledgments

The authors thank Alan Black, Tomáš Púčik, and an anonymous reviewer for providing comments on earlier drafts of this manuscript.

7. References

Atkins, N. T. and Wakimoto, R. M.: Wet microburst activity over the southeastern United States: Implications for forecasting, Wea. Forecasting, 6, 470–482, doi:10.1175/1520-0434(1991)006<0470:WMAOTS>2.0.CO;2, 1991.

Benjamin, S. G., Dévényi, D., Weygandt, S. S., Brundage, K. J., Brown, J. M., Grell, G. A., Kim, D., Schwartz, B. E., Smirnova, T. G., Smith, T. L., and Manikin, G. S.: An hourly assimilation–forecast cycle: The RUC, Mon. Wea. Rev., 132, 495–518, doi:10.1175/1520-0493(2004)132<0495:AHACTR>2.0.CO;2, 2004.

Benjamin, S. G., Weygandt, S. S., Brown, J. M., Hu, M., Alexander, C. R., Smirnova, T. G., Olson, J. B., James, E. P., Dowell, D. C., Grell, G. A., Lin, H., Peckham, S. E., Smith, T. L., Moninger, W. R., Kenyon, J. S., and Manikin, G. S.: A North American hourly assimilation and model forecast cycle: The Rapid Refresh, Mon. Wea. Rev., 144, 1669–1694, doi:10.1175/MWR-D-15-0242.1, 2016.

Black, A. W. and Mote, T. L.: Characteristics of Winter-Precipitation-Related Transportation Fatalities in the United States, Wea. Climate Soc., 7, 133–145, doi:10.1175/WCAS-D-14-00011.1, 2015.

Black, A. W., Villarini, G., and Mote, T. L.: Effects of Rainfall on Vehicle Crashes in Six U.S. States, Wea. Climate Soc., 9, 53–70, doi:10.1175/WCAS-D-16-0035.1, 2017.

Bland, J. M. and Altman, D. G.: The odds ratio, BMJ, 320, 1468, 2000.

Blumberg, W. G., Halbert, K. T., Supinie, T. A., Marsh, P. T., Thompson, R. L., and Hart, J. A.: SHARPpy: An open source sounding analysis toolkit for the atmospheric sciences, Bull. Amer. Meteor. Soc., 98, 1625–1636, doi:10.1175/BAMS-D-15-00309.1, 2017.

Cerniglia, C. S. and Snyder, W. R.: Development of warning criteria for severe pulse thunderstorms in the Northeastern United States using the WSR-88D. National Weather Service, Albany, NY, 2002.

Craven, J. P. and Brooks, H. E.: Baseline climatology of sounding derived parameters associated with deep, moist convection, Natl. Wea. Dig, 28, 13-24, 2004.

Fleiss, J. L., Levin, B., and Paik, M. C.: Statistical Methods for Rates and Proportions, Wiley, 2003.

Gensini, V. A., Mote, T. L., and Brooks, H. E.: Severe-thunderstorm reanalysis environments and collocated radiosonde observations, J. Appl. Meteor. Climatol., 53, 742–751, doi:10.1175/JAMC-D-13-0263.1, 2014.

Guillot, E. M., Smith, T. M., Lakshmanan, V., Elmore, K. L., Burgess, D. W., and Stumpf, G. J.: Tornado and severe thunderstorm warning forecast skill and its relationship to storm type, New Orleans, LA, 20–24 January 2008 2008.

Hamlington, B. D., Leben, R. R., Nerem, R. S., and Kim, K. Y.: The effect of signal-to-noise ratio on the study of sea level trends, J. Climate, 24, 1396-1408, doi:10.1175/2010JCLI3531.1, 2010.

Hurlbut, M. M. and Cohen, A. E.: Environments of Northeast U.S. severe thunderstorm events from 1999 to 2009, Wea. Forecasting, 29, 3-22, doi:10.1175/WAF-D-12-00042.1, 2013.

James, R. P. and Markowski, P. M.: A numerical investigation of the effects of dry air aloft on deep convection, Mon. Wea. Rev., 138, 140–161, doi:10.1175/2009MWR3018.1, 2010.

Johns, R. H. and Doswell, C. A. I.: Severe local storms forecasting, Wea. Forecasting, 7, 588–612, doi:10.1175/1520-0434(1992)007<0588:SLSF>2.0.CO;2, 1992.

505 Kingsmill, D. E. and Wakimoto, R. M.: Kinematic, dynamic, and thermodynamic analysis of a
506 weakly sheared severe thunderstorm over northern Alabama, Mon. Wea. Rev., 119, 262–
507 297, doi:10.1175/1520-0493(1991)119<0262:KDATAO>2.0.CO;2, 1991.
508 Lee, J. W.: Tornado proximity soundings from the NCEP/NCAR reanalysis data, M.S., Dept. of
509 Meteorology, University of Oklahoma, 61 pp., 2002.
510 McCann, D. W.: WINDEX - a new index for forecasting microburst potential, Wea. Forecasting,
511 9, 532–541, doi:10.1175/1520-0434(1994)009<0532:WNIFFM>2.0.CO;2, 1994.
512 Mesinger, F., DiMego, G., Kalnay, E., Mitchell, K., Shafran, P. C., Ebisuzaki, W., Jović, D.,
513 Woollen, J., Rogers, E., Berbery, E. H., Ek, M. B., Fan, Y., Grumbine, R., Higgins, W., Li,
514 H., Lin, Y., Manikin, G., Parrish, D., and Shi, W.: North American regional reanalysis,
515 Bull. Amer. Meteor. Soc., 87, 343–360, doi:10.1175/bams-87-3-343, 2006.
516 Miller, P. and Mote, T.: A climatology of weakly forced and pulse thunderstorms in the Southeast
517 United States, J. Appl. Meteor. Climatol., 56, 3017–3033,
518 doi:https://doi.org/10.1175/JAMC-D-17-0005.1, 2017.
519 Miller, P. W., Black, A. W., Williams, C. A., and Knox, J. A.: Quantitative assessment of human
520 wind speed overestimation, J. Appl. Meteor. Climatol., 55, 1009–1020,
521 doi:10.1175/JAMC-D-15-0259.1, 2016.
522 Moore, J. T. and Pino, J. P.: An interactive method for estimating maximum hailstone size from
523 forecast soundings, Wea. Forecasting, 5, 508–525, doi:10.1175/1520-
524 0434(1990)005<0508:AIMFEM>2.0.CO;2, 1990.
525 Murphy, M.: Preliminary results from the inclusion of lightning type and polarity in the
526 identification of severe storms, 8th Conf. on the Meteor. Appl. of Lightning Data, Seattle,
527 WA, 1–12, 2017.

Noel, J. and Dobur, J. C.: A pilot study examining model-derived precipitation efficiency for use in precipitation forecasting in the eastern United States, Natl. Wea. Dig., 26, 3–8, 2002.

Púčik, T., Groenemeijer, P., Rýva, D., and Kolář, M.: Proximity soundings of severe and nonsevere thunderstorms in Central Europe, Mon. Wea. Rev., 143, 4805–4821, doi:10.1175/MWR-D-15-0104.1, 2015.

Roberts, R. D. and Wilson, J. W.: A proposed microburst nowcasting procedure using single-Doppler radar, J. Appl. Meteor., 28, 285–303, doi:10.1175/1520-0450(1989)028<0285:APMNPU>2.0.CO;2, 1989.

Stewart, S. R.: The prediction of pulse-type thunderstorm gusts using vertically integrated liquid water content (VIL) and the cloud top penetrative downdraft mechanism. NOAA, 1991.

Sutton, R. T. and Hodson, D. L. R.: Climate response to basin-scale warming and cooling of the North Atlantic Ocean, J. Climate, 20, 891-907, doi:10.1175/JCLI4038.1, 2007.

Taszarek, M., Brooks, H. E., and Czernecki, B.: Sounding-derived parameters associated with convective hazards in Europe, Mon. Wea. Rev., 145, 1511-1528, doi:10.1175/MWR-D-16-0384.1, 2017.

Thompson, R. L., Edwards, R., Hart, J. A., Elmore, K. L., and Markowski, P.: Close proximity soundings within supercell environments obtained from the Rapid Update Cycle, Wea. Forecasting, 18, 1243–1261, doi:10.1175/1520-0434(2003)018<1243:CPSWSE>2.0.CO;2, 2003.

Thompson, R. L., Mead, C. M., and Edwards, R.: Effective storm-relative helicity and bulk shear in supercell thunderstorm environments, Wea. Forecasting, 22, 102–115, doi:10.1175/WAF969.1, 2007.

Thompson, R. L., Smith, B. T., Dean, A. R., and Marsh, P. T.: Spatial Distributions of Tornadic Near-Storm Environments by Convective Mode, Electronic J. Severe Storms Meteor., 8, 1–22, 2014.

Trenberth, K. E.: Signal versus noise in the Southern Oscillation, Mon. Wea. Rev., 112, 326-332, doi:10.1175/1520-0493(1984)112<0326:SVNITS>2.0.CO;2, 1984.

Ward, J. H.: Hierarchical grouping to optimize an objective function, Journal of the American Statistical Association, 58, 236–244, doi:10.1080/01621459.1963.10500845, 1963.

Weiss, S. J., Hart, J., and Janish, P.: An examination of severe thunderstorm wind report climatology: 1970–1999, 21st Conf. Severe Local Storms, San Antonio, TX, 446–449, 2002.

Wheeler, M. and Spratt, S. M.: Forecasting the potential for central Florida microbursts. NOAA, 1995.

Wolfson, M.: Characteristics of microbursts in the continental United States, Lincoln Lab Journal, 1, 49–74, 1988.

Appendix A.

Table A1. Additional detail describing the convective parameters in Table 2.

Parameter	Comments
MLCAPE	Mean-layer parcel mixed over the lowest 100 hPa
MLCIN	
MLLCL	
MLLFC	
MLEL	
NCAPE	MLCAPE / MLEL
K_IND	$T_{850} - T_{500} + T_{d850} - (T_{700} - T_{d700})$
TT	CT + VT
CT	$T_{d850} - T_{500}$
VT	$T_{850} - T_{500}$
PW	Depth of liquid water if all water vapor were condensed from the sounding
HGT0	Pressure level of the 0°C isotherm
ApWBZ	Height above ground level of the RAP pressure level with the wet bulb temperature nearest to 0°C
W_LOW	Mean mixing ratio between 1000–850 hPa
W_MID	Mean mixing ratio between 850–500 hPa
RH_LOW	Mean RH between 1000–850 hPa
RH_MID	Mean RH between 850–500 hPa
ThE_LOW	Mean theta-e from 1000–850 hPa
ThE_MID	Mean theta-e from 850–500 hPa
ML_BRN	Bulk Richard Number of the mean-layer parcel
Tc	Temperature of parcel lowered dry adiabatically from the convective condensation level
PEFF	As defined by Noel and Dobur (2002). PEFF equals the product of PW and the mean 1000–700-hPa RH.
DCAPE	Downdraft CAPE with respect to parcel with the minimum 100 hPa layer-averaged theta-e found in the lowest 400 hPa of the sounding.
WNDG	(MLCAPE)/2000*(0–3-km lapse rate)/9*(1–3.5-km mean wind)/15*[(MLCIN + 50)/40)]. Values larger than 1 indicate an increased risk for strong outflow gusts.
TEI	Difference between the surface theta-e and the minimum theta-e value in the lowest 400 hPa AGL
MICROB	Weighted sum of the following individual parameters: surface theta-e, SBCAPE, surface-based lifted index, 0–3-km lapse rate, VT, DCAPE, TEI, and PW. Values exceeding 9 indicate that microbursts are likely.
SWEAT	$12(T_{d850}) + 20(TT - 49) + 2(U_{850}) + (U_{500}) + 125[\sin(U_{dir500} - U_{dir850}) + 0.2]$
0-3-km_SHR	Magnitude of vector shear between surface and 3 km AGL
0-6-km_SHR	Magnitude of vector shear between surface and 6 km AGL
0-8-km_SHR	Magnitude of vector shear between surface and 8 km AGL
EBWD	Magnitude of vector shear between effective inflow base and one half of the MU equilibrium level height

Tables

Table 1. Kinematic and thermodynamic parameters of 1200-UTC composite soundings from Atlanta, Ga., USA, for each radar-identified morphological type in Miller and Mote (2017). Morphological types classified as WFTs are bolded. All kinematic values are shown in m s^{-1} whereas the units of the thermodynamic parameters are provided in the table. Explanations for the variable abbreviations can be found in Table 1 and Appendix A.

Type	0–6-km _SHR	0–8-km _SHR	0–12-km Max Wind	0–12-km Mean Wind	ThE _LOW (K)	MLCAPE (J kg^{-1})	Forecast SBCAPE (J kg^{-1})
1	**4.3**	**5.1**	**7.2**	**3.0**	**343.0**	**562**	**1585**
2	**4.3**	**5.1**	**8.8**	**3.6**	**341.9**	**365**	**1214**
3	**4.7**	**6.2**	**9.4**	**3.7**	**340.5**	**289**	**1176**
4	**4.3**	**5.7**	**8.3**	**3.7**	**341.1**	**357**	**1121**
5	**3.2**	**5.1**	**9.6**	**3.2**	**341.7**	**283**	**1006**
6	6	7.7	11.6	5.0	339.0	211	973
7	8.2	10.8	16.5	6.1	336.6	66	723
8	4.9	7.7	13.6	3.1	336.0	24	558
9	5.4	8.7	15.4	3.0	330.6	0	32
10	7.9	9.8	13.5	5.8	334.5	0	391

578 **Table 2.** List of the 31 convective parameters computed from the proxy soundings where CAPE,
579 CIN, LCL, LFC, and EL and correspond to convective available potential energy, convective
580 inhibition, lifted condensation level, level of free convection, and equilibrium level, respectively.

Abbrev.	Full Name	Units
MLCAPE	Mean-layer CAPE	J kg^{-1}
MLCIN	Mean-layer CIN	J kg^{-1}
MLLCL	Mean-layer LCL	m
MLLFC	Mean-layer LFC	m
MLEL	Mean-layer EL	m
NCAPE	Normalized MLCAPE	m s^{-2}
K_IND	K index	°C
TT	Total totals	°C
CT	Cross totals	°C
VT	Vertical Totals	°C
PW	Precipitable Water	mm
HGT0	Height of 0°C temperature isotherm	hPa
ApWBZ	Approximate height of 0°C wet bulb temperature	m
W_LOW	Mean low-level mixing ratio	g kg^{-1}
W_MID	Mean mid-level mixing ratio	g kg^{-1}
RH_LOW	Mean low-level relative humidity	--
RH_MID	Mean mid-level relative humidity	--
ThE_LOW	Mean low-level theta-e	K
ThE_MID	Mean mid-level theta-e	K
ML_BRN	Mean layer bulk Richardson number	--
Tc	Convective temperature	°C
PEFF	Precipitation efficiency	--
DCAPE	Downdraft CAPE	J kg^{-1}
WNDG	Wind damage parameter	--
TEI	Theta-e index	°C
MICROB	Microburst composite index	--
SWEAT	Severe weather and threat index	--
0-3-km_SHR	0–3-km vertical wind shear	m s^{-1}
0-6-km_SHR	0–6-km vertical wind shear	m s^{-1}
0-8-km_SHR	0–8-km vertical wind shear	m s^{-1}
EBWD	Effective layer vertical wind shear	m s^{-1}

581

582 **Table 3.** RAP error statistics for surface-based CAPE (SBCAPE) and several of the variables listed
583 in Table 2. The statistics are presented similarly to Thompson et al. (2003) by providing the mean
584 RAP-derived value, the mean arithmetic error (bias), and the mean absolute error (MAE).

Parameter	Mean	Bias	MAE	R^2
SBCAPE	1354.3	141.3	530.4	0.59
MLCAPE	943.4	112.6	338.0	0.64
MLLCL	1077.4	-32.9	151.8	0.82
Total Totals	44.8	0.51	1.54	0.74
TEI	21.1	-2.30	3.80	0.69
0–3-km Shear	6.33	-0.48	1.38	0.82
0–6-km Shear	8.39	-0.28	1.40	0.88

585

586 **Table 4.** WFT, SWS, and SHS day frequency by radar site.

Site	WFT Days	Wind Control	SWS Days	% SWS	Hail Control	SHS Days	% SHS
KAKQ	376	351	25	6.6	363	13	3.5
KAMX	581	569	12	2.1	575	6	1.0
KBMX	376	364	12	3.2	372	4	1.1
KCAE	401	339	62	15.5	377	24	6.0
KCLX	450	407	43	9.6	440	10	2.2
KDGX	426	403	23	5.4	416	10	2.3
KEOX	384	366	18	4.7	382	2	0.5
KEVX	467	449	18	3.9	463	4	0.9
KFCX	408	318	90	22.1	370	38	9.3
KFFC	400	358	42	10.5	387	13	3.3
KGSP	417	334	83	19.9	383	34	8.2
KGWX	362	349	13	3.6	354	8	2.2
KHPX	299	282	17	5.7	294	5	1.7
KHTX	373	343	30	8.0	369	4	1.1
KJAX	555	520	35	6.3	546	9	1.6
KJGX	384	356	28	7.3	377	7	1.8
KLIX	504	492	12	2.4	501	3	0.6
KLTX	452	439	13	2.9	444	8	1.8
KMHX	497	496	1	0.2	495	2	0.4
KMLB	540	532	8	1.5	532	8	1.5
KMOB	451	444	7	1.6	446	5	1.1
KMRX	415	349	66	15.9	384	31	7.5
KMXX	357	346	8	2.2	350	4	1.1
KNQA	356	336	20	5.6	345	11	3.1
KOHX	349	336	13	3.7	345	4	1.1
KPAH	330	305	25	7.6	318	12	3.6
KRAX	367	337	30	8.2	355	12	3.3
KTBW	546	525	21	3.8	535	11	2.0
KTLH	482	461	21	4.4	479	3	0.6
KVAX	457	430	27	5.9	452	5	1.1
Mean	425	398	27	6.7	415	10	2.5

587

588 **Table 5.** Summary of convective parameters on SWS days. The "Sites" column indicates the
589 number of spatial subdivisions within which the difference between the SWS mean and the control
590 mean was accompanied by $p < 0.10$; the "percent change" column shows the relative increase or
591 decrease of the mean on SWS days.

Parameter	Sites	Percent change
VT	28	5.1
TT	27	4.2
MLCAPE	25	31.2
MICROB	23	44.0
DCAPE	22	17.3
TEI	22	13.1
MLLCL	21	12.9
ThE_LOW	21	0.9
RH_LOW	20	-5.5
WNDG	19	41.2
CT	19	3.2
Tc	19	5.8
MLEL	18	8.0
SWEAT	14	7.8
W_LOW	10	3.0
K_IND	8	3.8
RH_MID	7	-3.2
ThE_MID	6	0.1
PEFF	6	-3.8
0-6-km_SHR	6	-4.5
0-8-km_SHR	6	-6.5
ApWBZ	5	-0.5
HGT0	4	0.1
W_MID	3	0.0
MLBRN	3	-0.7
NCAPE	2	23.9
PW	2	0.9
0-3-km_SHR	2	-1.2
MLCIN	0	6.6
MLLFC	0	0.9
EBWD	0	-1.9

592

593 **Table 6.** Same as Table 5, except for SHS days.

Parameter	Sites	Percent change
VT	27	8.0
TT	27	7.5
CT	21	7.1
PEFF	16	-11.0
MLLCL	15	13.2
HGT0	14	2.4
ApWBZ	14	-6.0
RH_LOW	14	-5.3
DCAPE	13	23.3
MLCAPE	12	28.8
PW	12	-6.7
W_MID	11	-9.2
ThE_MID	10	-0.7
WNDG	10	27.4
RH_MID	9	-7.8
TEI	7	10.4
MICROB	7	21.6
SWEAT	7	10.1
W_LOW	6	-2.1
Tc	6	3.2
0-6-km_SHR	6	9.7
0-8-km_SHR	5	6.9
MLEL	4	3.8
K_IND	3	2.7
ThE_LOW	3	-0.1
0-3-km_SHR	3	5.3
NCAPE	1	27.0
MLCIN	1	17.7
MLLFC	1	4.1
MLBRN	1	-15.8
EBWD	1	9.5

594

595 **Figures**

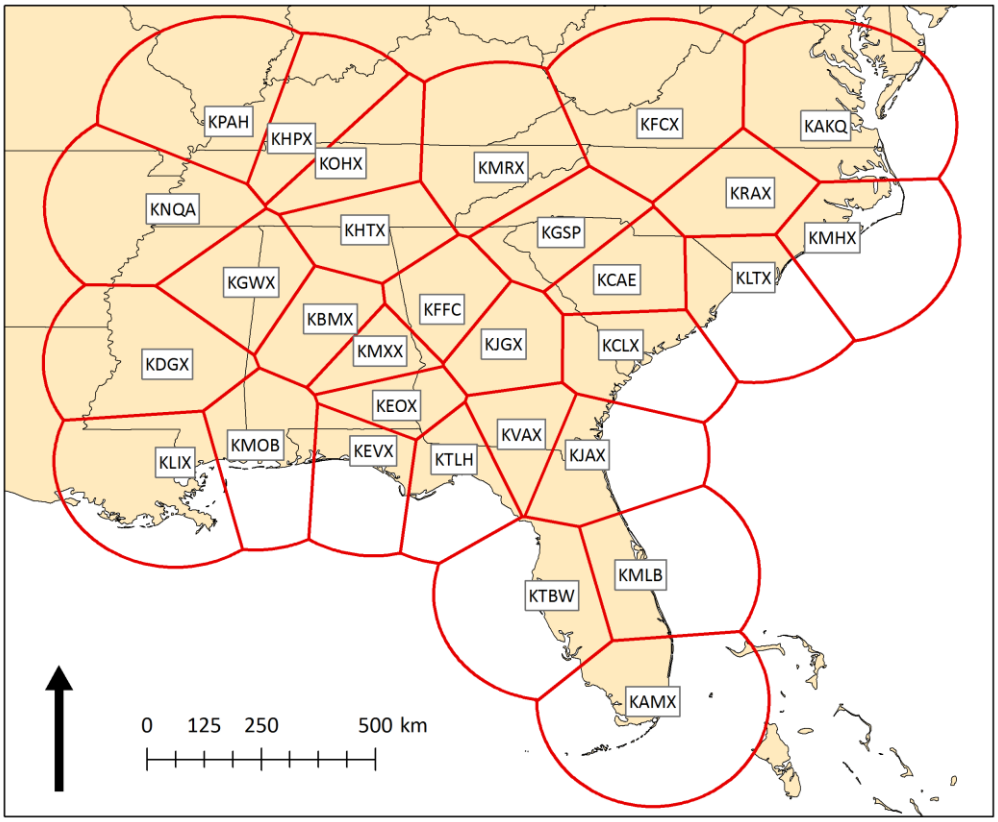

596

597 **Figure 1**. WSR-88D sites contributing to the Miller and Mote (2017) WFT climatology.

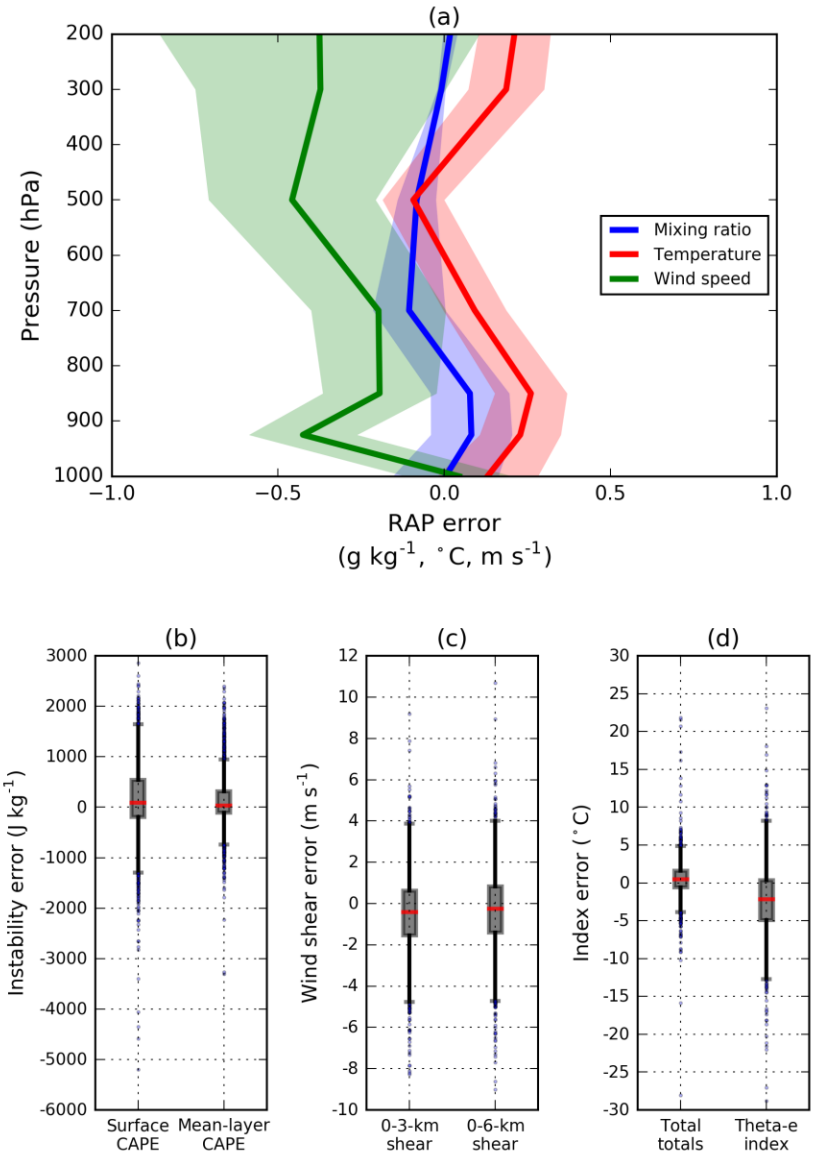

Figure 2. Vertical profiles of RAP output errors measured by co-located radiosonde observations (a). Errors were calculated at 1000, 925, 850, 700, 500, 300, and 200 hPa. The 95% confidence interval for the mean error (solid lines) is shaded. Boxplots of the resulting error for six derived quantities is shown in (b)-(d). The interquartile range (IQR), representing the middle 50% of values, is depicted by the gray box. Values lying more than 1.5*IQR from the median (red line) are marked with dots.

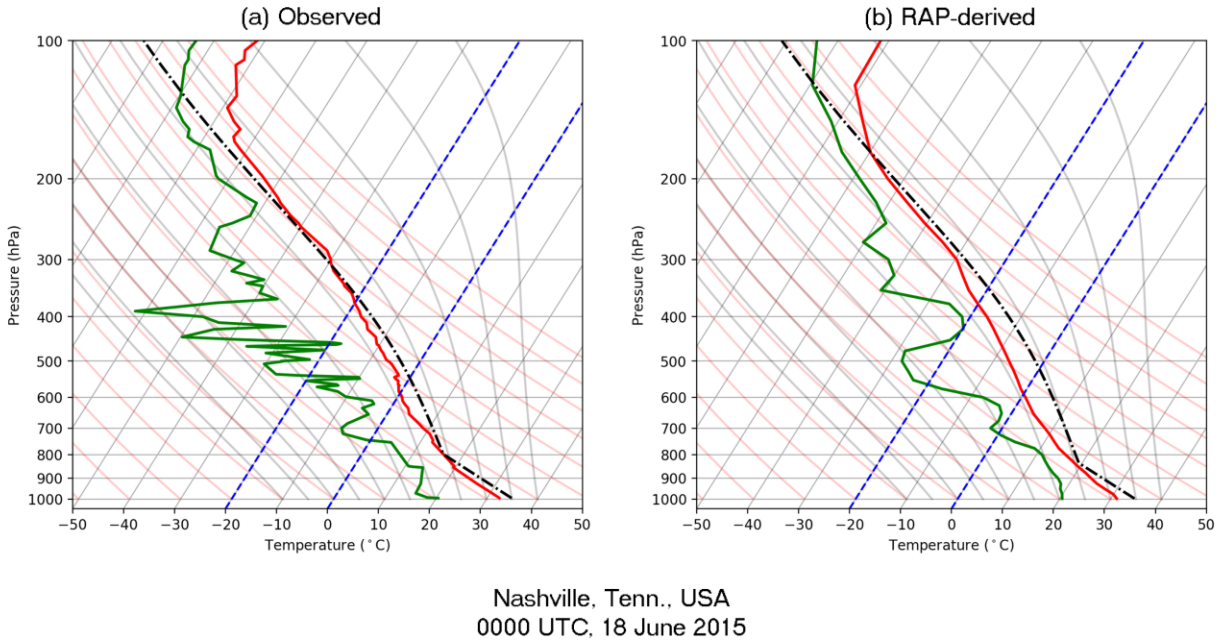

605

606 **Figure 3.** Comparison of observed (a) versus RAP-derived (b) soundings for a case when the
607 MLCAPE discrepancy exceeded 1000 J kg^{-1} (observed: 1028 J kg^{-1}; RAP: 2051 J kg^{-1}). Minor
608 mischaracterizations of low-level moisture contributed to a large response in MLCAPE during the
609 vertical integration of the parcel trajectory.

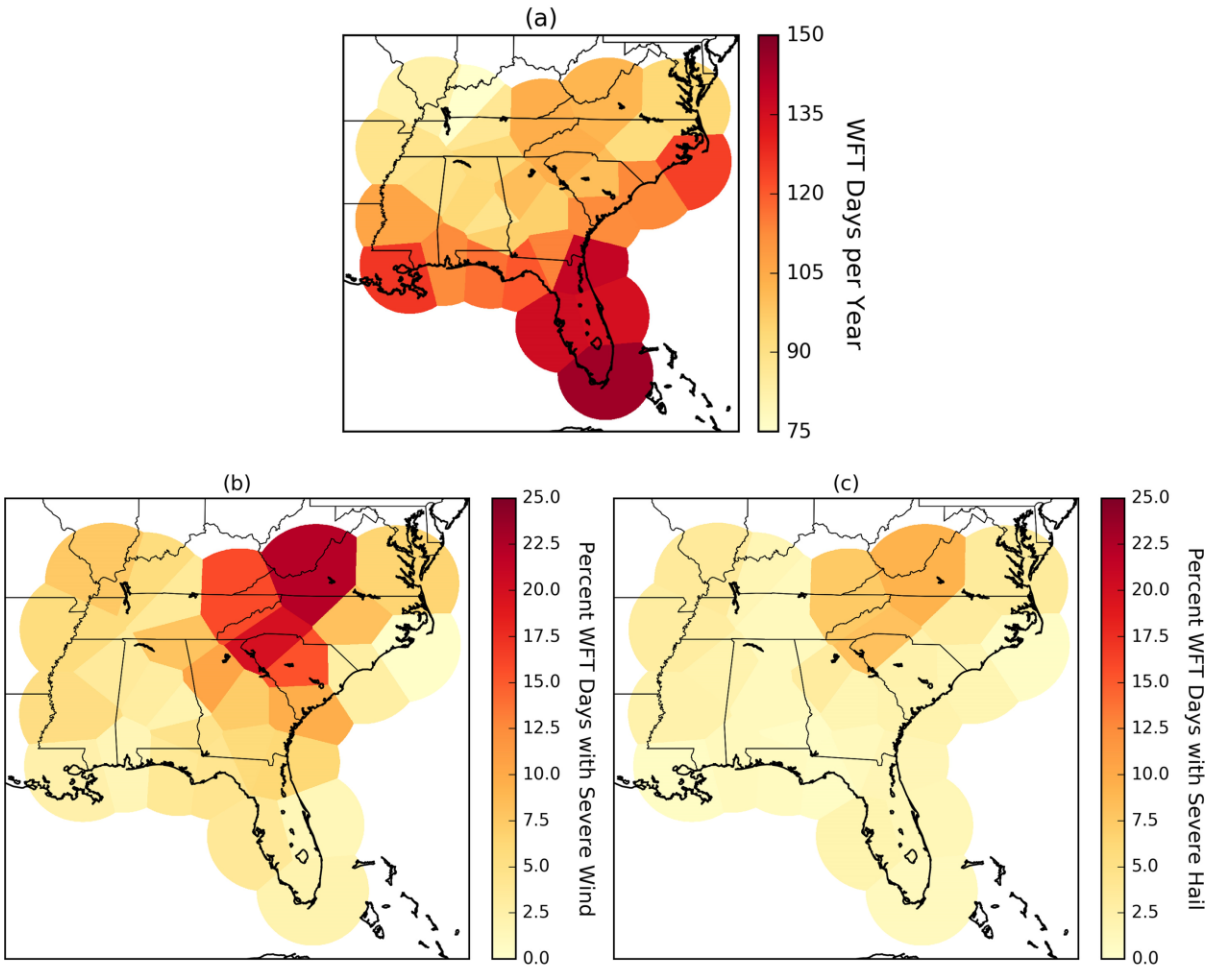

610

611 **Figure 4.** Average number of WFT days during the four-year study period (a) compared to the

612 proportion of WFT days affiliated with severe wind (b) and severe hail (c) events.

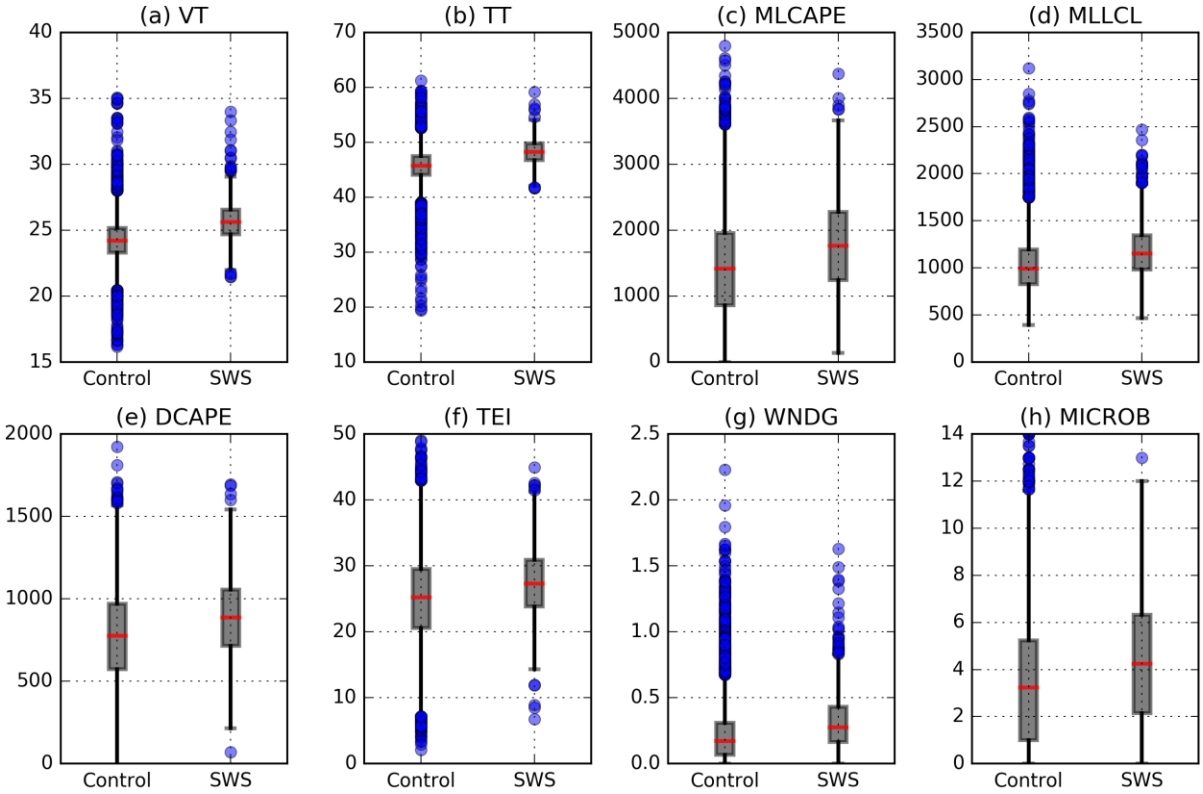

613

614 **Figure 5.** Boxplots of selected convective parameters that demonstrated skill in differentiating

615 between the control days and SWS days.

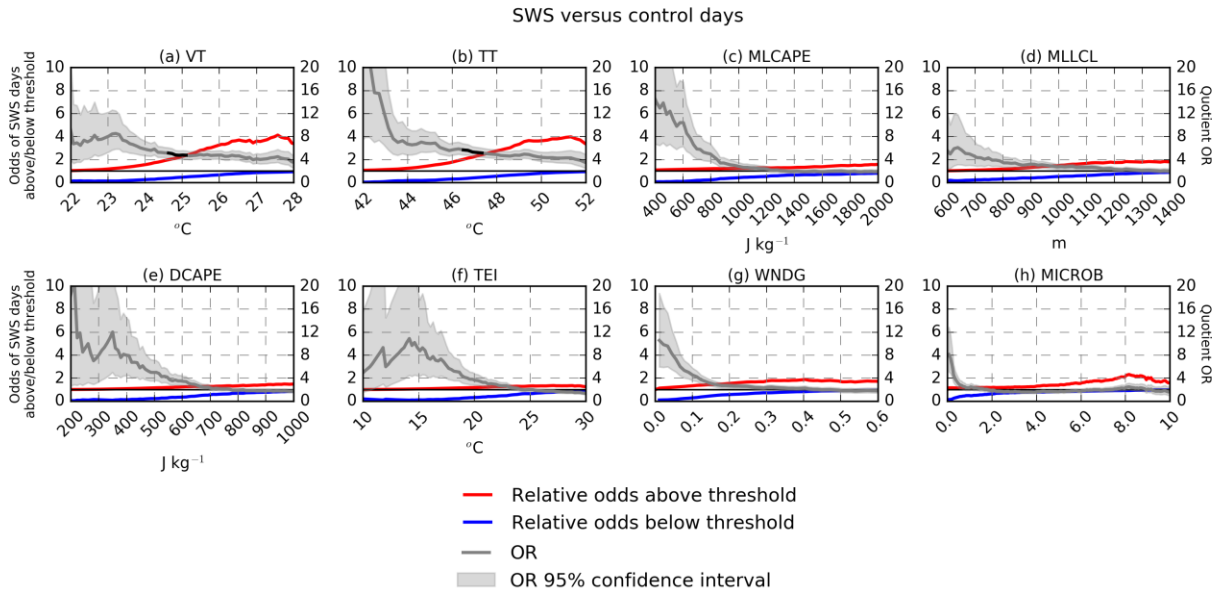

616

617 **Figure 6.** ORs for the same eight convective parameters shown in Fig. 5. Whenever the OR,
618 defined by Eq. (2), results from a numerator (red) ≥2 and a denominator (blue) ≤0.5, then the OR
619 is drawn in black. The left y-axis expresses values corresponding to the OR's numerator and
620 denominator (red and blue lines), and the right y-axis corresponds to the OR value (gray line). At
621 very low and very high threshold values, the variance of the OR may be undefined, and the 95%
622 OR confidence interval cannot be computed.

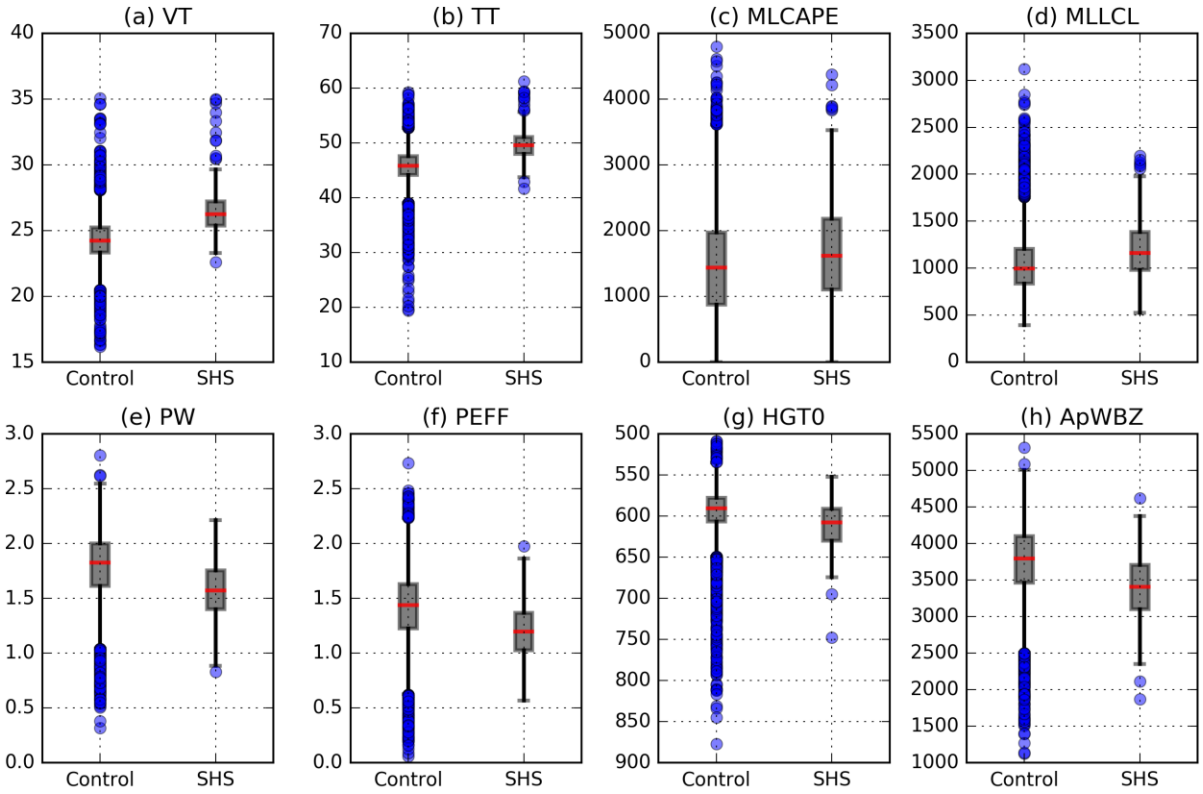

623

624 **Figure 7.** Same as Fig. 5 except for SHS days. Panes (a)-(d) replicate the same variables shown in

625 Fig. 5 whereas (e)-(h) are replaced with four SHS-specific parameters from Table 6.

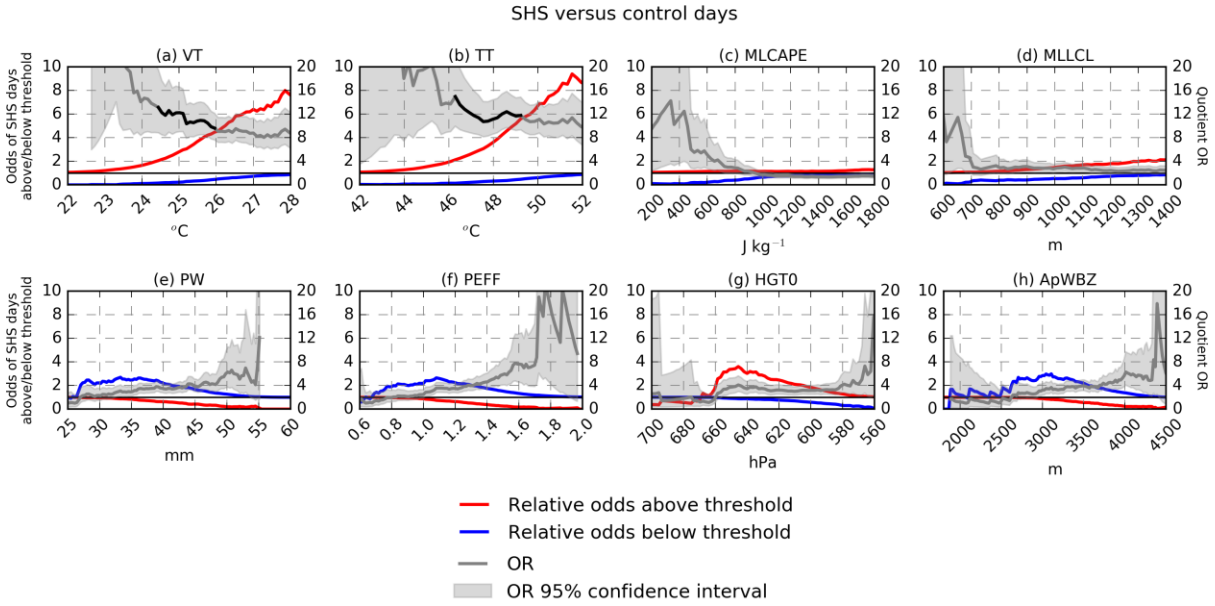

626

627 **Figure 8.** Same as Fig. 6 except for SHS days. Panes (a)-(d) replicate the same variables shown in
628 Fig. 6 whereas (e)-(h) are replaced with four SHS-specific parameters from Table 6. At very low
629 and very high threshold values, the variance of the OR may be undefined, and the 95% OR
630 confidence interval cannot be computed.

631

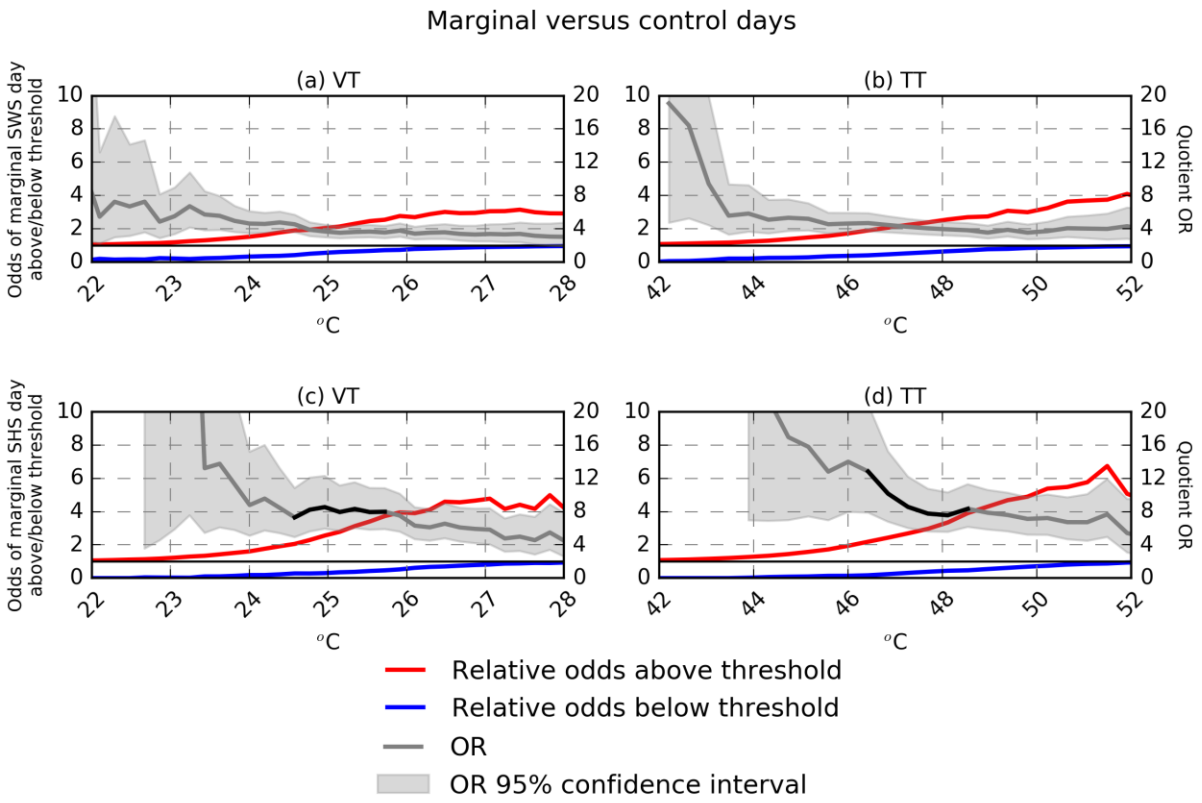

632

633 **Figure 9.** Same as Fig. 6a-b (a-b) and Fig. 8a-b (c-d) except that only marginal SWS and SHS

634 days are used to calculate the OR. At very low and very high threshold values, the variance of the

635 OR may be undefined, and the 95% OR confidence interval cannot be computed.